Bioorganic Chemistry 89 (2019) 103008

Contents lists available at ScienceDirect

Bioorganic Chemistry

journal homepage: www.elsevier.com/locate/bioorg

Biosynthesized silver nanoparticles for inhibition of antibacterial resistance and biofilm formation of methicillin-resistant coagulase negative *Staphylococci*

Govindan Rajivgandhi[a,d], Muthuchamy Maruthupandy[b,c,*], Thillaichidambaram Muneeswaran[b,c], Muthusamy Anand[c], Franck Quero[b], Natesan Manoharan[d], Wen-Jun Li[a]

[a] State Key Laboratory of Biocontrol and Guangdong Provincial Key Laboratory of Plant Resources, School of Life Sciences, Sun Yat-Sen University, Guangzhou 510275, PR China

[b] Laboratorio de Nanocelulosa y Biomateriales, Departamento de Ingeniería Química, Biotecnología y Materiales, Facultad de Ciencias Físicas y Matemáticas, Universidad de Chile, Avenida Beauchef 851, Santiago, Chile

[c] Department of Marine and Coastal Studies, Madurai Kamaraj University, Madurai 625 021 Tamil Nadu, India

[d] Department of Marine Science, Bharathidasan University, Tiruchirappalli, Tamil Nadu 620024, India

ARTICLE INFO

Keywords:
Silver nanoparticles
Biological synthesis
Multidrug resistant bacteria
Antibiofilm activity
Methicillin-resistant coagulase negative *Staphylococci*

ABSTRACT

The ability of a natural stabilizing and reducing agent on the synthesis of silver nanoparticles (Ag NPs) was explored using a rapid and single-pot biological reduction method using *Nocardiopsis* sp. GRG1 (KT235640) biomass. The UV–visible spectral analysis of Ag NPs was found to show a maximum absorption peak located at a wavelength position of ~422 nm for initial conformation. The major peaks in the XRD pattern were found to be in excellent agreement with the standard values of metallic Ag NPs. No other peaks of impurity phases were observed. The morphology of Ag NPs was confirmed through TEM observation, demonstrating that the particle size distribution of Ag NPs entrenched in spherical particles is in a range between 20 and 50 nm. AFM analysis further supported the nanosized morphology of the synthesized Ag NPs and allowed quantifying the Ag NPs surface roughness. The synthesized Ag NPs showed significant antibacterial and antibiofilm activity against biofilm positive methicillin-resistant coagulase negative *Staphylococci* (MR-CoNS), which were isolated from urinary tract infection as determined by spectroscopic methods in the concentration range of 5–60 μg/ml. The inhibition of biofilm formation with coloring stain was morphologically imaged by confocal laser scanning microscopy (CLSM). Morphological alteration of treated bacteria was observed by SEM analysis. The results clearly indicate that these biologically synthesized Ag NPs could provide a safer alternative to conventional antibiofilm agents against uropathogen of MR-CoNS.

1. Introduction

Multidrug resistance (MDR) bacteria are an emerging burden and represent a daily challenge for the management of antimicrobial therapy in healthcare settings [1]. Therefore, there is an emerging need to discover effective, secure and affordable antimicrobial agents to handle this problem. Silver and its derivatives are being utilized owing to their antimicrobial ability for infections caused by microbes [2]. Most researchers reported that silver nanoparticles (Ag NPs) possess efficient antibacterial activity against Gram-positive (GP) and Gram-negative (GN) MDR bacterial strains [3]. In addition to MDR, many bacteria create a community like structure designated as biofilm, which embedded in a complex polymer matrix of several bacterial cells, adapt to live in apprehensive conditions and develop resistance to current antibiotics [4]. The biofilm formations defend the bacterial cells when compared with free-living cells. In particular, the biofilm forming bacteria play a major role in urinary tract infection (UTIs) and may cause death [5]. Among UTI pathogens, GP bacteria *Staphylococci aureus* is frequently present in the mixed population of biofilm and it is related to UTI obstruction, blockage of urinary catheters and kidney infections [6]. It also linked to other related infections like catheter association including crystalline biofilms, urinary stones, pyelonephritis, and septicemia [7]. Hence, current researchers are investigating novel strategies and chemical compounds to compete with the biofilm

* Corresponding author at: Laboratorio de Nanocelulosa y Biomateriales, Departamento de Ingeniería Química, Biotecnología y Materiales, Facultad de Ciencias Físicas y Matemáticas, Universidad de Chile, Avenida Beauchef 851, Santiago, Chile. Tel.: +56 936415260.
E-mail address: mmaruthupandy@yahoo.in (M. Maruthupandy).

https://doi.org/10.1016/j.bioorg.2019.103008
Received 29 March 2019; Received in revised form 18 May 2019; Accepted 20 May 2019
Available online 21 May 2019
0045-2068/

inhibition role, which quickly develops resistance.

Nanotechnology is emanating as an expeditious increasing field with its application in science and technology for the purpose of producing new materials that possess nanoscale dimensions [8]. The synthesis of nanoparticles via biological methods is very reliable and is an alternative to more complex chemical synthetic procedures to obtain nanomaterials. Some of these biological methods include the use of microbes and plants extract [9–11]. In addition, most of the chemicals used to synthesize NPs are hazardous for the environment and living organisms [12,13]. Various categories of nanomaterials like metal, metal oxide and polymer NPs have recently arisen from biologically mediated syntheses [14,15]. Among these nanoparticles, Ag NPs were found to be more productive and applied for many applications including antimicrobials, therapeutics, anti-biofilm, anticancer, biomolecular detection, biolabeling, catalysis and microelectronics, nonlinear optics and intercalation materials for electrical batteries [16–20]. In particular, the excellent antimicrobial efficacy of Ag NPs due to their special physicochemical properties have been reported.

Marine actinomycete is an important resource for obtaining new products for healthcare and other industrial applications that are of potential interest for the synthesis of antimicrobial agents [21]. The production of Ag NPs by using marine actinomycetes could potentially offer improved stability and reduced polydispersity due to extreme and unexplored environments, which was predicted to be a rich source of novel metabolites. Previously, marine actinomycetes were found to possess significant biocidal activity against MDR pathogens [22,23]. The present study aimed to synthesize and characterize Ag NPs using marine actinomycete of *Nocardiopsis* sp. GRG1 (KT235640) as biological stabilizing and reducing agent. In addition, the antibiofilm activity and their potential effects against GP bacterial strain of methicillin-resistant coagulase negative *staphylococci* (MR-CoNS) was investigated.

2. Materials and methods

2.1. Preparation of actinomycetes biomass

Nocardiopsis sp. GRG1 (KT235640) was inoculated into starch casein broth medium, previously prepared with 50% of seawater and incubated at 28 °C for 6 days in a shaker at 120 rpm. The culture was centrifuged at 5000 rpm at 4 °C for 15 min and the deposited mycelium was subsequently stored at 4 °C after consecutive washing with distilled water [24].

2.2. Biological synthesis of Ag NPs

In brief, ~20 g of *Nocardiopsis* sp. GRG1 (KT235640) biomass was transferred to 100 ml of 1 mM silver nitrate ($AgNO_3$) solution and incubated at 28 °C for 6 days in a shaker at 120 rpm. The flask was ascertained for the visible color change from yellow to brown at regular interval. The experimental actions were carried out under dark condition. After the incubation, the solution was centrifuged at 5000 rpm for 30 min and the pellets were collected.

2.3. Characterization of Ag NPs

The UV–visible absorption spectrum (Shimadzu UV-2500) of Ag NPs was recorded using the absorption mode and in the wavelength range of 200–800 nm. Fourier transform infrared spectroscopy (FTIR, NEXUS-870) of synthesized Ag NPs was performed in the wavenumber range of 4000–400 cm^{-1} and the KBr disc method was used for recording the spectra. XRD patterns of the samples in a powder form were recorded at a voltage of 40 kV, a current of 30 mA, 2θ range from 30° to 80° in a fixed time mode at room temperature using a XPERT-PRO X-ray diffractometer equipped with Cu Kα radiation (λ = 1.54178 Å). The roughness factor of the Ag NPs was measured by atomic force microscopy (AFM, SU-70 ModelL-hi-0028-0001). Structural morphology characterization of Ag NPs was imaged by transmission electron microscopy (TEM) (Hitachi JEM-2100).

2.4. Specimen collection

The retrospective study was performed from November 2017 to December 2017 at K. A. P. V. Government Medical College & Hospital, Tiruchirappalli, Tamil Nadu, India. A total of 100 urine specimens were obtained for 1 month from 55-year-old men using sterile container.

2.5. Isolation and identification of bacterial strain

The urine specimens were streaked on biplates, including 5% sheep blood agar (BA)/MacConkey agar (MCA). All the plates were incubated at 37 °C for 24 h. After incubation, the presence and absence of the colonies in the plates was observed based on the hemolysis and pigment production [25]. Consequently, the positive cultures were streaked on bile esculin plates for *Enterococci* sp. and mannitol salt agar (MSA) for *Staphylococci* sp. Based on the color and hemolysis variation of MSA was used as a specific agar for *Staphylococci* sp.

2.6. Detection and characterization of CoNS strain

The isolates were identified by catalase and tube coagulase tests. If the isolates were confirmed as CoNS, biochemical tests and antimicrobial discs were used for their characterization up to species level. All the procedure was used according to Bergey's manual [26].

2.7. Antimicrobial susceptibility pattern (ASP)

The antibiotic resistance of CoNS strain was determined using specific UTI panel for *staphylococci* including HX UTI 012 & HX UTI 077 antibiotic discs method, imipenom (IPM-10 μg), azlreonam (AT-30 μg), cefoperazone/sulbactum (CFS-75/10 μg), piperacill/tazobactam (PIT-100/10 μg), ceftazidime (CAZ-30 μg), netillin (NET-30 μg) and amoxyclav (AMC-30 μg), ampicillin (AMP-10 μg), ciproflaxacin (Cip-5 μg), co-Trimoxazole (Cot-25 μg), gentamicin (Gen-10 μg), norfloxacin (NX-10 μg) respectively. The control strain of *S. aureus* ATCC 25923 was also used for comparison [27].

2.8. Detection of methicillin resistant uropathogens

The detection of methicillin resistance effect in the control *S. aureus* ATCC 25923 and selected CoNS was conducted by Kirby-Bauer disk-diffusion method [28]. Around the methicillin, third generation cephalosporin antibiotics including ceftazidime, cefotaxime, ceftazidime/clavulanic acid, ceftazidime/clavulanic acid were also used for this study.

2.9. Identification of biofilm formation

The detection of biofilm formation in MR-CoNS was performed by quantitative tissue culture plate method (TCP) [29]. Briefly, the 24 h cultures of MR-CoNS were cultivated in 96-well polystyrene plate (Himedia, India) supplemented with 0.1% glucose as the growth medium, combined with tryptic soy broth (TSB) at 37 °C for 24 h. After incubation, all the wells were washed with 0.2 ml of phosphate buffered saline (PBS) to detach the non-adhering cells. 0.1% crystal violet solution (w/v) staining was subsequently applied for 15 min and the cells were fixed with 9% ethanol. A non-biofilm producer of *S. aureus* ATCC 25923 was used as a positive control, which was evaluated at a wavelength of 600 nm by spectrophotometry. The isolates are designated as biofilm positive > 0.240 and all the experiment was performed in triplicate. Based on the CLSI Guidelines, the values of biofilm positive and negative are reported in Table 1.

Table 1
CLSI Guideline of biofilm detection for Gram-negative bacteria and Gram-positive bacteria. OD stands for optical density.

Biofilm formation	Adherence	Mean value of OD
High	Strong	> 0.240
Moderate	Moderate	0.120–0.240
Non/Weak	Non/Weak	< 0.120

2.10. Congo red agar assay (CRA)

The selected isolate was streaked on the CRA plates and incubated at 37 °C for 24 h. The MR-CoNS biofilm promoter strain exhibited dark black color colonies and the non-biofilm producer of *S. aureus* ATCC 25923 exhibited red colonies. The slight pink color indicated the absence of dry crystalline morphology; while black color colonies produced a darkening, which represents the variation of dry crystalline morphology [30].

2.11. Antibacterial activity

The antibacterial activity of the Ag NPs was determined by agar well diffusion method against the growth of MR-CoNS with the third-generation cephalosporin ceftazidime as the reference drug, and the zones of inhibition around the various concentrations were measured. Inhibition zones ≥8 mm were considered indicative of inhibitory activity [31].

2.12. Antibiofilm activity

The Ag NPs were evaluated against biofilm positive MR-CoNS using 24-well microtiter plates [32]. Briefly, the 1% of 24 h cultures were inoculated in 24-well microtitre plates containing TSB incorporated with 5–60 µg/ml of Ag NPs at 37 °C for 24 h. After incubation, the biofilm was stained with 0.4% crystal violet solution (w/v) for 5 min after washing with distilled water and air dried. Finally, 1 ml of ethanol was added, and the OD value was determined at 600 nm by ELIZA reader. The absence of Ag NPs containing wells acted as control TSB alone served as a blank. The experiments were performed in triplicates. The percentage of inhibition (PI) was calculated using the following formula:

$$PI = [(\text{Control OD 600 nm} - \text{Test OD 600 nm})/\text{Control OD 600 nm}] \times 100$$

where OD stands for optical density at 600 nm.

2.13. Confocal laser scanning electron microscope (CLSM)

The colloidal damage of the sticky cells was assessed by CLSM [33]. The 24 h lag phase culture of biofilm positive MR-CoNS was inoculated in sterile TSB and the cells were treated with 55 µg/ml of Ag NPs. The plates were incubated at 37 °C for 24 h. After incubation, the centrifuged cells were washed three times with phosphate buffer solution (PBS). 1 mg/ml concentration of acridine orange (AO) was used for detection of live and dead cells variation in dark condition. The treated and untreated cells were analyzed by CLSM using a 488 nm argon laser and a 500–640 nm band pass emission filter.

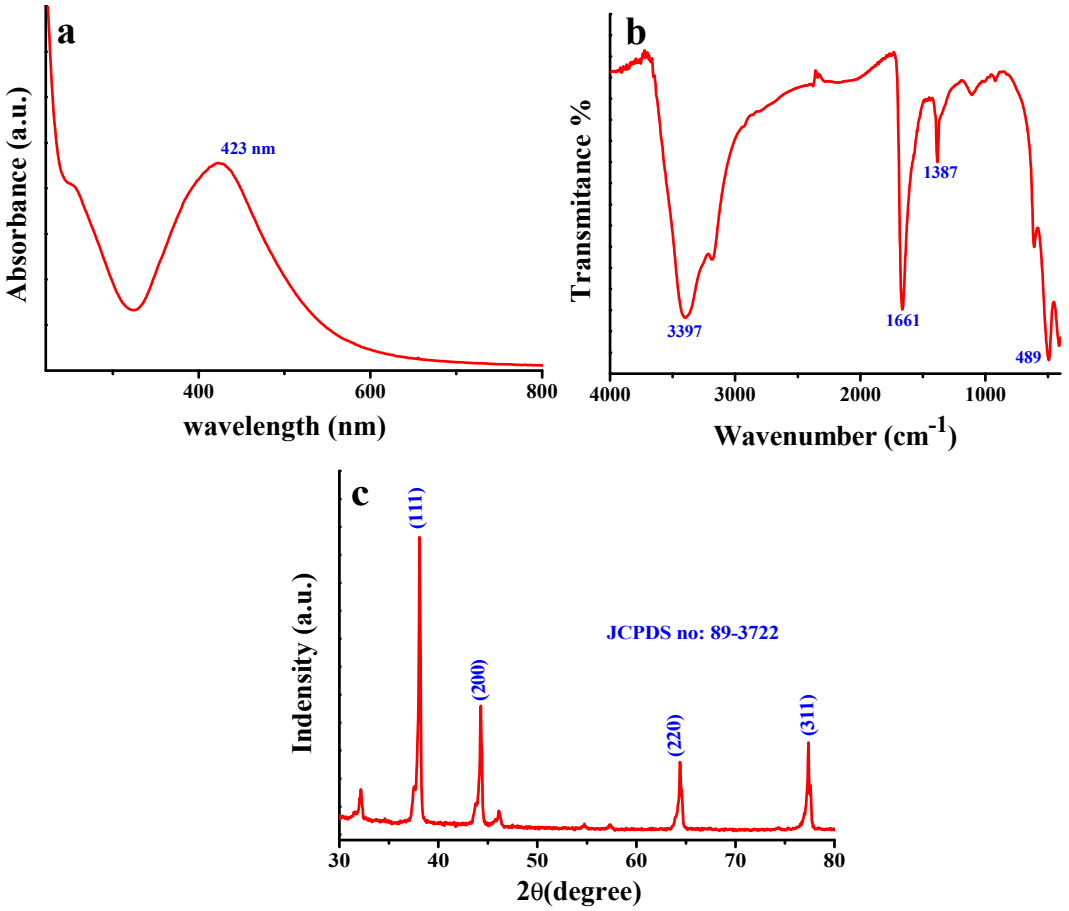

Fig. 1. (a) UV–visible spectrum in the wavelength range of 200–800 nm, (b) FTIR spectrum in the wavenumber range of 4500–400 cm^{-1} and (c) powder XRD pattern in the 2θ diffraction angle range of 10°–80°, for Ag NPs.

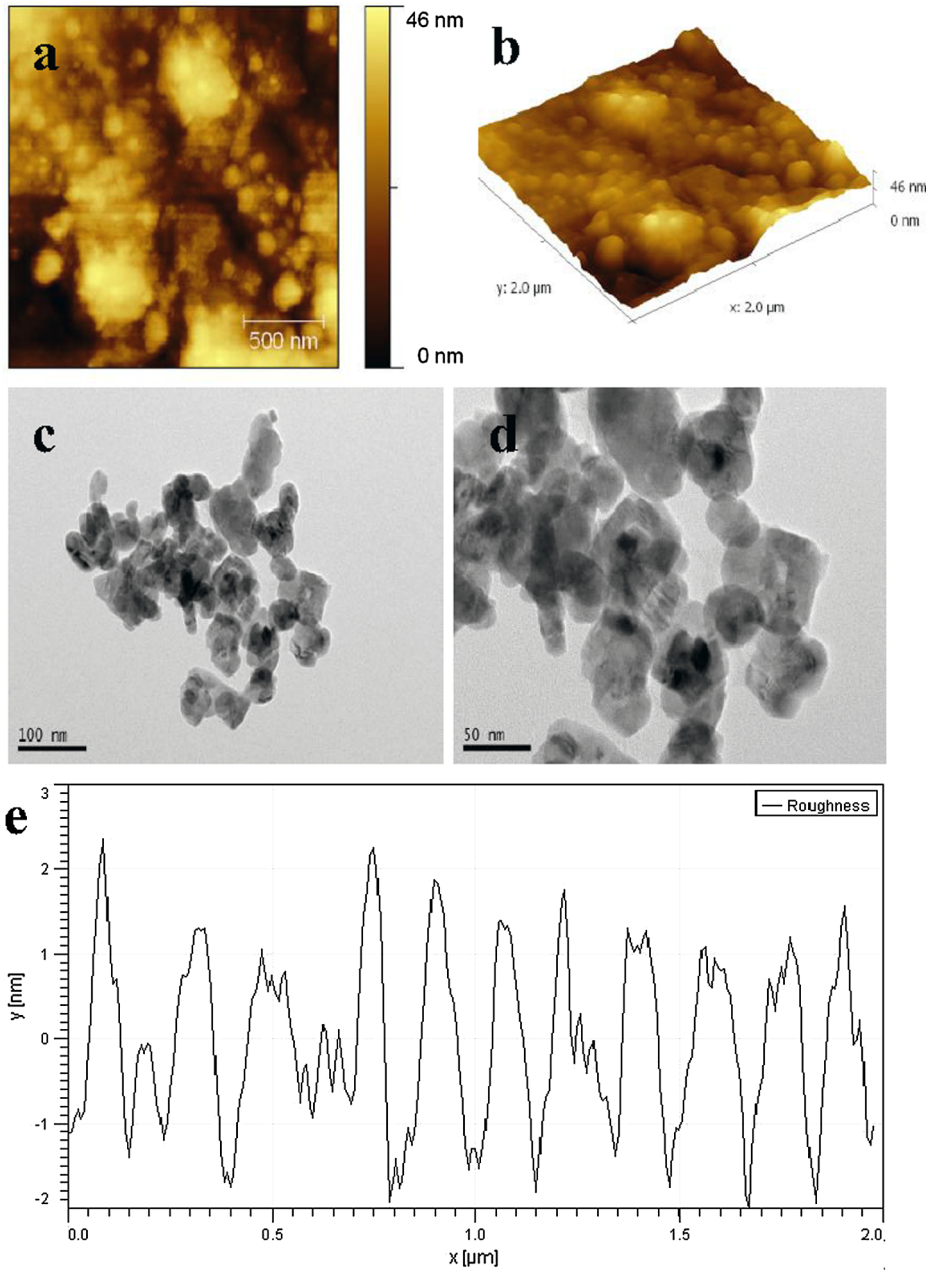

Fig. 2. AFM images obtained in (a) height mode, (b) in orthogonal projection from height mode. TEM micrographs obtained at (c) low and (d) high magnification. (e) Graph showing the roughness of Ag NPs.

2.14. Scanning electron microscopy (SEM)

The ability of Ag NPs to alter the surface morphology of biofilm positive MR-CoNS was visualized by SEM [34]. The centrifuged cells were treated with BIC 55 µg/ml of Ag NPs in 10 mM PBS (pH 7.4), incubated for 24 h at 37 °C. After incubation, the cells were fixed with an equal volume of 4% glutaraldehyde. The fixed cells were vacuum filtered onto a 0.1 mm polycarbonate membrane filters and dehydrated through a graded series of ethanol (10, 20, 30, 40, 50, 60, 70, 80, 90 and 100%). The filters were then dried and mounted onto aluminum specimen supports and coated with a 15 nm thickness of gold–-palladium metal (60:40 alloy). The samples were examined using a Cambridge Stereo scan 200 SEM using an accelerating voltage of 20 kV.

3. Results and discussion

3.1. Characterization of Ag NPs

The UV–visible spectrum of Ag NPs synthesized using *Nocardiopsis* sp. GRG1 (KT235640) biomass is shown in Fig. 1a. The UV–visible spectrum displays a strong surface plasmon resonance band at a wavelength of ~423 nm due to the inter-band shift and plasmon movement of the NPs and sharp peak, which are known to be related to the size and shape of Ag NPs [35]. The surface plasmon resonance band typically shifts towards higher wavelength positions upon changes in NPs size [36]. This detection is in agreement with the qualitative analysis of Ag NPs.

FTIR analysis was carried out to further confirm the synthesis of Ag NPs in the presence of biomass of *Nocardiopsis* sp. GRG1 (KT235640). A

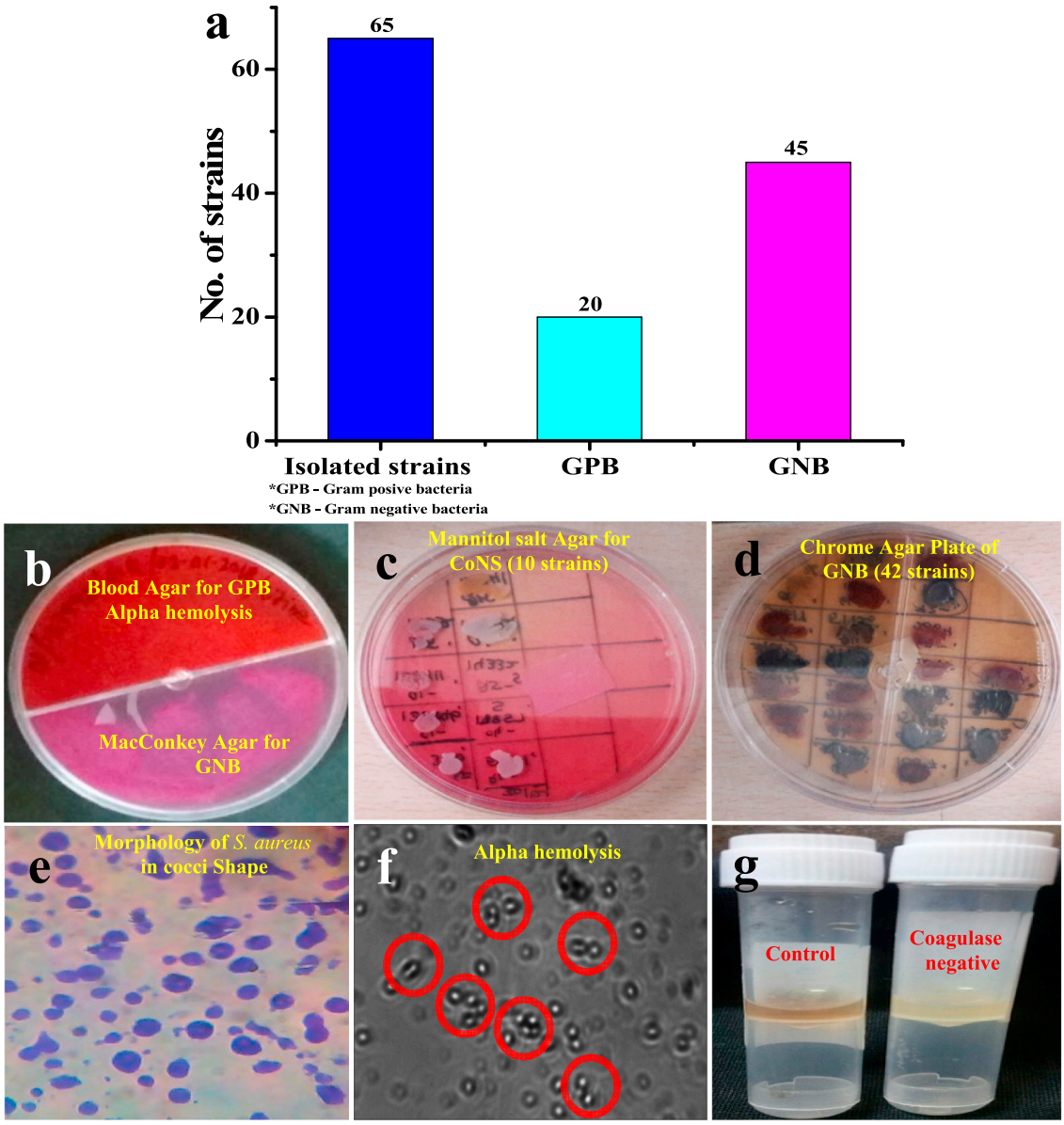

Fig. 3. (a) Isolation of uropathogens, including 20 hemolytic (GPB) and 45 lactose-fermenting colonies (GNB), (b) screening of CoNS strain among UTI infections, isolation of GPB and GNB in biplate method, (c) screening of GPB in MSA agar, (d) screening of GNB in chrome agar plate, (e), morphological observation of *Staphylococci* sp. and identification of coagulase negative result in (f) phase contrast microscope and (g) plasma tube.

typical FTIR spectrum analysis for Ag NPs is reported in Fig. 1b, highlighting four important absorption peaks located at wavenumber positions of ~3397, 1661, 1387 and 489 cm^{-1}, respectively. The broad peak located at a wavenumber position of ~3441 cm^{-1} corresponds to N—H stretching motions of amides. The peak at located at a wavenumber position of ~1643 cm^{-1} is also attributed to the vibrational motions related to N—H binding of amines and the small peak located at a wavenumber position of ~617 cm^{-1} is related to the vibrational motions of C-Cl moieties in alkyl halides. The peak located at a wavenumber position of ~1643 cm^{-1} suggests that amide and amine bonding may participate in the stabilization of Ag NPs (see Fig. 1b), which may play an essential role in the capping mechanism of Ag NPs [37].

The examination of the crystalline structure of Ag NPs was carried out by powder XRD. The XRD pattern of Ag NPs is shown in Fig. 1c. The 2θ values of ~38.0°, 44.4°, 64.3° and 77.4° correspond to the (1 1 1), (2 0 0), (2 2 0) and (3 1 1) reflection planes, respectively. This indicates that the Ag NPs possess a spherical shape and are crystalline in nature (JCPDS file no: 89-3722). Some additional small peaks located at 2θ positions of ~32.2° and 46.2° indicate the presence of bioorganic compounds/proteins occurring at the surface of the Ag NPs during synthesis [38]. These bioorganic compounds reflecting peaks were weaker than that corresponding to the crystalline structure present in Ag NPs. The powder XRD pattern corresponding to Ag NPs display the reflection planes typical for a face-centered cubic form of metallic silver. No other peaks were observed, which suggests the high purity of the synthesized Ag NPs [39,40].

AFM was used to observe the Ag NPs surface morphology and size. The corresponding images are reported in Fig. 2a,b. The two-dimensional image of the Ag NPs demonstrated that the NPs possess a spherical morphology (Fig. 2a). The size of the Ag NPs was measured using the size measurement tool of the AFM software and their diameter size was found to be between 30 and 50 nm. The three-dimensional image allowed revealing the roughness factor of Ag NPs and providing information on the morphology homogeneity of the NPs (Fig. 2b). Ag NPs were also examined using TEM analysis, which further confirmed that

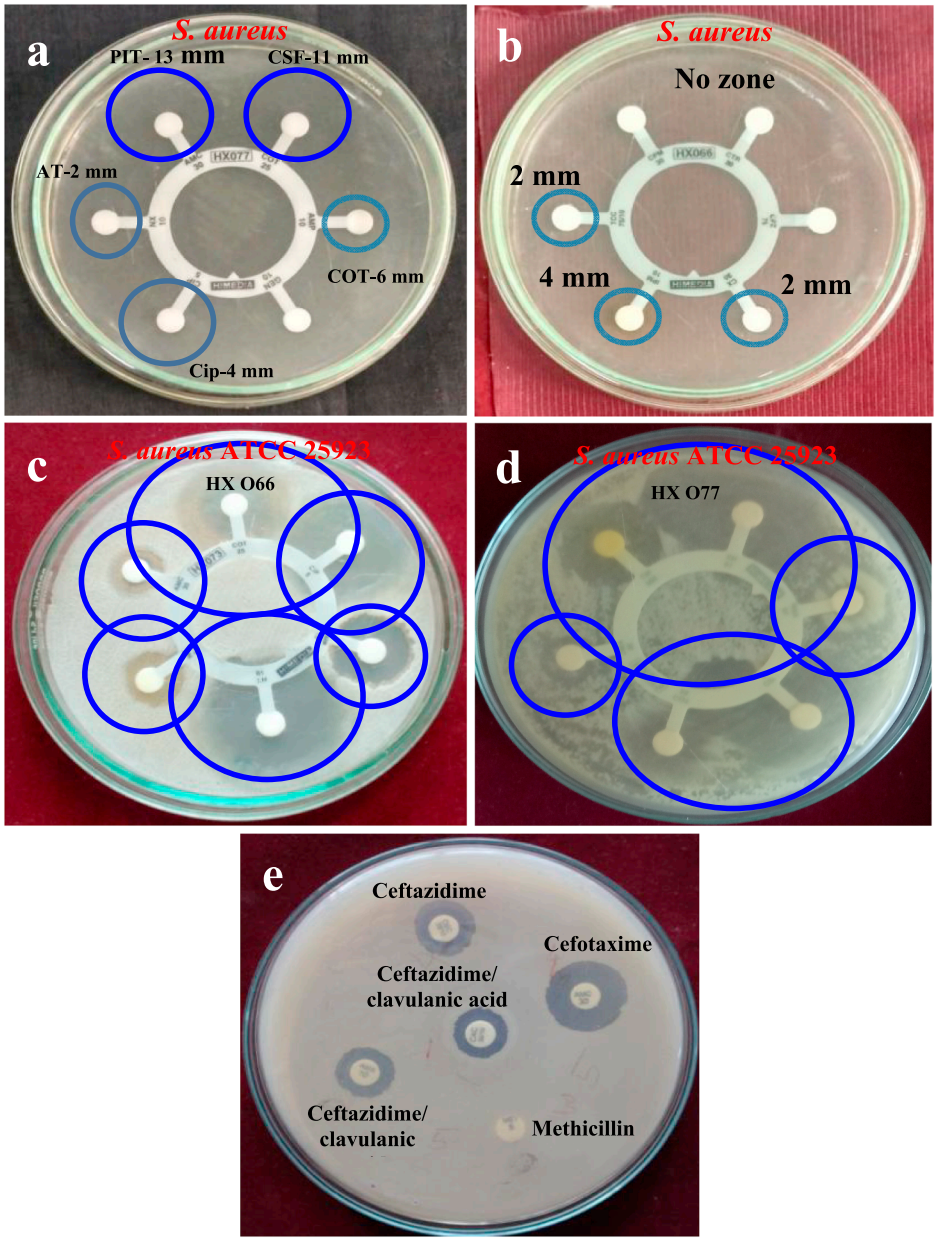

Fig. 4. Multidrug resistant effect of CoNS strain by UTI panel (a) HX 066 (a), (b) HX 077 discs method, control strain of *S. aureus* ATCC 25923 tested by (c) HX 066, (d) HX 077 and (e) detection of methicillin resistant CoNS strain against various third generation cephalosporin along with methicillin.

Ag NPs possess a size ranging from 20 to 50 nm. Also, the images suggested that the NPs were relatively well-dispersed and spherical in morphology, as shown in Fig. 2c,d. Additionally, the particle size distribution further revealed that most of Ag NPs possess a 35 nm diameter size, demonstrating that actinomycetes strain allows obtaining smaller Ag NPs with potentially high surface area. The roughness of Ag NPs was quantified by AFM. Values of maximum roughness peak height (R_p) of 2.32 nm, average maximum roughness (R_{pm}) peak height of 1.90 nm, maximum roughness valley depth (R_v) 1.99 nm and average maximum roughness valley depth (R_{vm}) of 1.72 nm were obtained for these Ag NPs (Fig. 2e).

3.2. Isolation of uropathogens

Among the 100 samples, 65 strains were isolated in biplate (Fig. 3b), including 20 hemolytic and 45 lactose-fermenting colonies (Fig. 3a). Based on their observation, the isolated colonies were inoculated with their respective media plates including BA and MSA for GPB (Fig. 3c) and chrome agar (CA) for GNB (Fig. 3d). Out of 20 strains of GPB, 10 numbers of alpha hemolytic *Staphylococcus* sp. were screened from MSA plates and the morphology of *S. aureus* (Fig. 3e) and alpha hemolysis (Fig. 3f) was observed by phase contrast microscopy (Fig. 3f). The catalase positive (Fig. 3g) and coagulase negative results were confirmed, and the isolates were CoNS, which differed from other GPB, including *Entrococcus* sp. and *Staphylococci* sp. After 4 h interval of coagulase negative, results revealed that 10 strains showed coagulase negative and were named as CoNS.

3.3. Antimicrobial susceptibility pattern (ASP)

Among the 10 CoNS, 7 strains developed resistance against UTI panel of HX 066 and HX 077 discs. The selected strains exhibited 4, 2, 2 mm zone against HX 077 and 13, 11, 6, 4 and 2 mm zone against CIP, AMC, COT, and NX of HX 066 were observed, respectively. The control

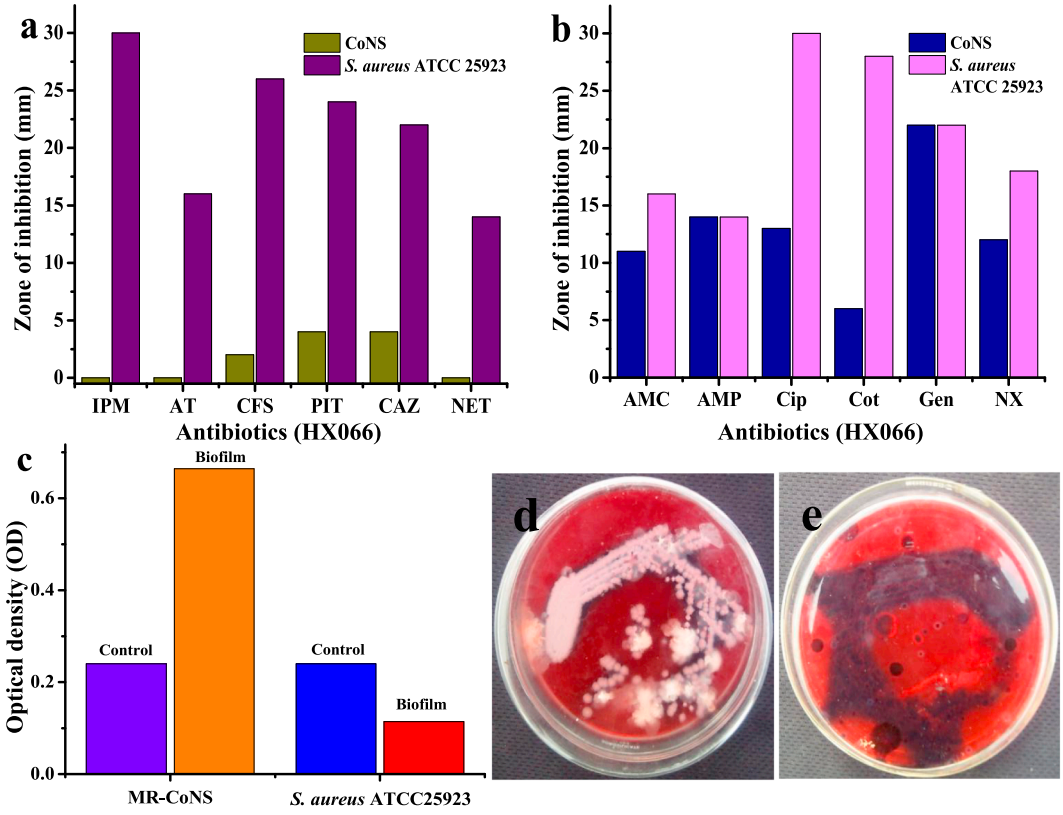

Fig. 5. The comparison of zone against CoNS and *S. aureus* ATCC 25923 by using (a) HX 066 and (b) HX 077. Detection of biofilm formation by (c) TCA method and (d,e) CRA method. (d) The pink color colonies plates revealed absence of exopolysaccharide production in *S. aureus* ATCC and (e) exopolysaccharide production of CoNS exhibited black color colonies.

Table 2
CLSI Guideline value of antibiotic zone against multi drug resistant (MDR) *S. aureus*.

Sample No	Antibiotics	CLSI guidelines of inhibition zone for MDRs of *S. aureus*			Test pathogens (MDR)
		S (mm)	I (mm)	R (mm)	
1	Ceftazidime (CAZ-30 μg)	21	18–20	17	*S. aureus*
2	Cefotaxime (CTX-30 μg)	26	23–25	22	*S. aureus*
3	Ciprofloxacin (Cip-5 μg)	21	16–20	15	*S. aureus*
4	Co-Trimoxazole (Cot-25 μg)	16	11–15	10	*S. aureus*
5	Gentamycin (GEN-10 μg)	15	13–14	12	*S. aureus*
6	Imipenom (IMP-10 μg)	23	20–22	19	*S. aureus*
7	Ceftazidime/clavulanic acid	24	22–24	22	*S. aureus*
8	Ceftazidime/clavulanic acid	29	24–26	22	*S. aureus*
9	Cefoperazone/sulbactum (CFS-75/10 μg)	20	17–19	21	*S. aureus*
10	Piperacill/tazobactam (PIT-100/10 μg)	22	13–16	13	*S. aureus*
12	Ampicillin (AMP-30 μg)	23	18–21	13	*S. aureus*
14	Ampicillin (AMP-10 μg)	22	22–23	16	*S. aureus*
15	Aztreonam (AT-10 μg)	18	14–17	13	*S. aureus*
16	Norfloxacin (NF-10 μg)	18	14–17	13	*S. aureus*
19	Methicillin				*S. aureus*
17	Netillin (NET-10 μg)	17	13–16	12	*S. aureus*
18	Amoxyclav (AMC-30 μg)	16	12–14	10	*S. aureus*

strains of *S. aureus* ATCC 25923 were found to be more sensitivity, including 24, 26, 22, 30, 16 and 14 mm and 30, 16, 28, 14, 12 and 22 mm against PIT, CSF, CAZ, IMP, AT and NET and CIP, AMC, COT, AMP, NX and GEN were observed (Fig. 4a–b), respectively. Based on the resistance against selected Hexa disc antibiotics of MR-CoNS, the results were compared with *S. aureus* ATCC 25923 and the comparison is presented in Fig. 4c,d. The zone variation of MR-CoNS was compared with *S. aureus* ATCC 25923 and the results are presented in Fig. 5a,b. This zone of inhibition did not reach the same inhibition level against selected CoNS as reported in the CLSI guidelines [41]. Our previous report evidenced that the partial zone producing ciprofloxacin and norfloxacin was sensitive to MDR pathogens and CoNS were the most recurrent urinary isolates [42]. Hence, the results suggest that the selected isolates developed resistance against all current antibiotics and confirmed why these are considered as MDR strains. The zone variation of *S. aureus* was compared with CLSI guidelines zone and the obtained results are presented in Tables 2 and 3.

3.4. Detection of methicillin-resistant CoNS strain

After 24 h incubation, the amoxicillin/clavulanic acid exhibited 11 mm zone of inhibition and ceftazidime/clavulanic acid, cefotaxime/

Table 3
The zone interpretation of HX 066 and HX 077 UTI panel discs against multi drug and methicillin resistant *S. aureus*. CoNS stands for coagulase-negative *staphylococci*. S, I and R stand for Sensitive, Intermediate and Resistant, respectively.

Antibiotics (HX066)	Zone of inhibition (mm)	
	CoNS	*S. aureus* ATCC 25,923
Imipenom (IPM)	No zone	30
Azlreonam (AT)	No zone	16
Cefoperazone/sulbactum (CFS)	2	26
Piperacill/tazobactam (PIT)	4	24
Ceftazidime (CAZ)	4	22
Netillin (NET)	No zone	14
Amoxyclav (AMC)	11	16
Ampicillin (AMP)	14	14
Ciproflaxacin (Cip)	13	30
Co-Trimoxazole (Cot)	6	28
Gentamicin (Gen)	22	22
Norfloxacin (NX)	12	18
Cefotaxime (CTX)	18	No zone
Cefotaxime (CTX)	16	–
Ceftazidime/clavulanic acid (CAC)	27	–
Cefotaxime/clavulanicacid (CEC)	14	–
Methicillin (MET)	0	No zone

Table 4
Confirmation of biofilm formation in *S. aureus* by UV–visible spectroscopy. OD stands for optical density.

Name of the isolates	Control	OD value	Biofilm production
MR-CoNS	≥0.240	0.664	Strong
S. aureus ATCC 25923	≤0.240	0.114	Weak

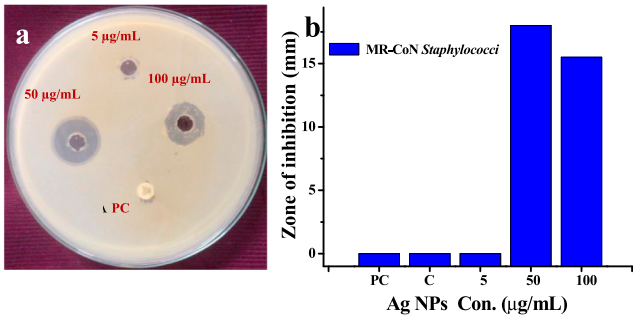

Fig. 6. Antibacterial activity of Ag NPs against (a) MR-CoNS plate and (b) graphical representation of antibacterial activity.

clavulanic acid and amoxicillin showed zones of inhibition of 6, 9, 7 mm respectively, whereas no zone of inhibition against methicillin was observed. However, the results revealed that the selected CoNS strains have methicillin resistance and revealed that MR-CoNS strains are comparatively more resistant to all antibiotics (Fig. 4e). Among the 50 isolates, 30 were resistant against methicillin as reported before from urinary isolates of CoNS [43]. *Staphylococcus* is the most frequent and dangerous uropathogens, which developed resistance against at least one drug due to improper prescription [44]. The present finding is in agreement with previous studies, which shows MR-CoNS as the most common in UTI.

3.5. Identification of biofilm formation

An OD value of 0.664 was obtained for MR-CoNS whereas the control *S. aureus* ATCC 25923 exhibited an OD value of 0.114 (Fig. 5c). The results, however, confirmed that the MR-CoNS pathogen is a biofilm producer (Table 4). Furthermore, the black color colonies of CRA plate indicated that the exopolysaccharides was synthesized by the selected strain (Fig. 5e). However, the selected strain was confirmed as a biofilm producer. The pink color colonies of the control strain (*S. aureus* ATCC 25923) confirmed their inability of biofilm production (Fig. 5d). Recently, Neupane et al. [30] documented that the ESBL producing GNB *E. coli* could produce biofilm formation in CRA plates and leads to recurrent infections in UTIs. The MDR strains of *P. mirabilis* and *E. coli* are biofilm producers due to exopolysaccharide synthesis as reported by Rajivgandhi et al. [6] using CRA method.

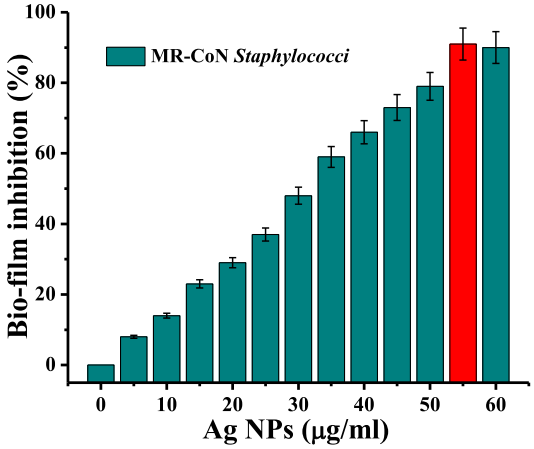

Fig. 7. Inhibition of biofilm formation by various concentrations of Ag NPs against MR-CoNS strain (average of three replicates). The error bars correspond to the standard deviation obtained the averages.

3.6. Antibacterial activity of Ag NPs

The evaluation of Ag NPs against MR-CoNS resulted in inhibition zones of 18 mm at 50 µg/ml and 15.5 mm at 100 µg/ml. As a result, no vast difference in the inhibition results were observed between concentrations of 50 and 100 µg/ml. Therefore, the highest inhibition concentration of 50 µg/ml was chosen for further invitro antibacterial activity study (Fig. 6a,b). The positive control of ceftazidime exhibited no zone of inhibition. Hence, this result clearly indicates that the synthesized Ag NPs effectively inhibit the bacteria and possess the strongest bactericidal activity. Our result agrees with an earlier finding by Manukumar et al. [45], which reported that biologically mediated Ag NPs was effective against food borne pathogens. Gupta et al. [46] also reported that the synthesized Ag NPs using actinomycete exhibited better inhibition against MDR pathogens. Hence, our result demonstrated that the Ag NPs synthesized in the presence of *Nocardiopsis* sp. GRG1 (KT235640) biomass is very effective against MR-CoNS, even at relatively low concentration (55 µg/ml).

3.7. Inhibition of biofilm formation

The synthesized Ag NPs were observed at their effective concentration (55 µg/ml), which resulted in 91% of inhibition against MR-CoNS using 24-well polystyrene plate (Fig. 7). The result revealed that the biofilm inhibition concentration (BIC) of Ag NP was fixed as 55 µg/ml. It proved that Ag NPs are more potent against biofilm colonization and cell adherences. In the future, Ag NPs could potentially be used for the treatment of infections caused by a highly antibiotic resistant biofilm [47] since it was documented that Ag NPs modulate the quorum quenching activity against *S. aureus* biofilm by 24 well plate. Previously, the actinomycete mediated metal NPs inhibited the biofilm formation of MDR pathogens at 100 µg/ml as reported by Mu et al. [48]. Hence, the Ag NPs synthesized in the present study perform better

Table 5
Previous report of concentration dependent nanoparticles against biofilm forming bacteria. MIC stands for minimum inhibitory concentration.

Sample	Test Organisms	Antibacterial activity (μg/mL)	MIC (μg/mL)	References
Ag NPs	*Mycrobaterium tuberculosis*	250	250	[49]
Ag NPs	*Pseudomonas aerugino*	100	100	[50]
Ag NPs	*Pseudomonas aeruginosa*	200	200	[51]
Ag NPs	*Streptococcus mutans*	100 ppm	100 ppm	[52]
Ag NPs	*Enterobacteriaceae*	200–250	250	[53]
Ag NPs	*Escherichia coli, Pseudomonas aeruginosa* and *Staphylococcus aureus*	65	65	[54]
Ag NPs	*Staphylococcu aureus* and *Pseudomonas aeruginosa*	50 and 100	50 and 100	[55]
Ag NPs	*Escherichia coli,* *Klebsiella pneumoniae, Pseudomonas aeruginosa, Proteus mirabilis* and *Acinetobacter baumannii*	75	75	[56]
Ag NPs	*Acinetobacter baumannii*	150	150	[57]
	Klebsiella aerogenes	150	150	
	Escherichia coli	150	150	
	Klebsiella pneumoniae	150	150	
	Pseudomonas	150	150	
	aeruginosa	150	150	
	Pantoea agglomerans	150	150	
	Proteus mirabilis	150	150	
	Staphylococcus aureus	150	150	
	Streptococcus pyogenes and	150	150	
	Salmonella typhi			
Ag NPs	Methicillin-resistant *Staphylococcus aureus*	55	55	**Present study**

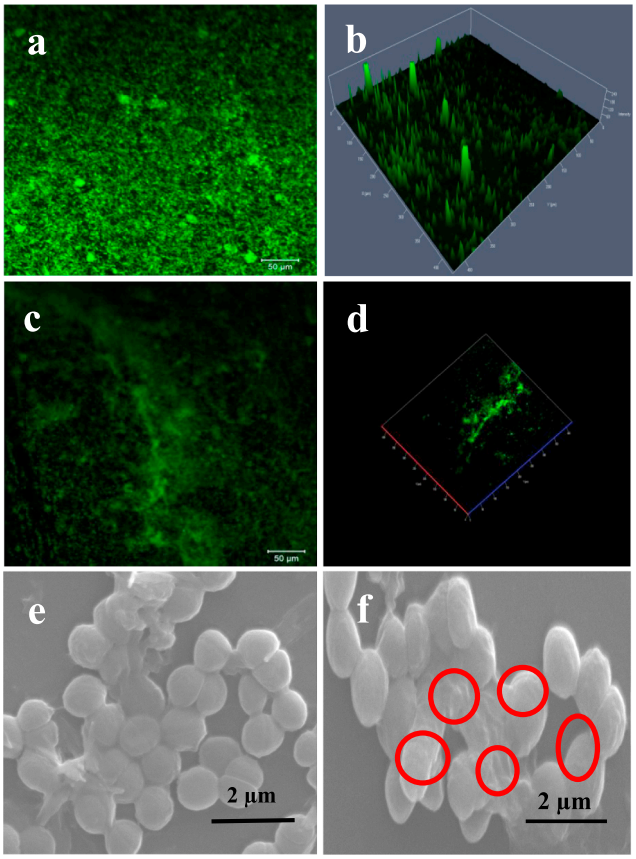

Fig. 8. Identification of live/dead cells of untreated MR-CoNS strain (a) 2D, (b) 3D and (c) Ag NPs treated MR-CoNS strain 2D, (d) 3D by CLSM. Morphological alteration of (e) untreated image of MR-CoNS strain and (f) Ag NPs treated MR-CoNS strain observed by SEM.

when compared with previous study (Table 5). Even a relatively low concentration of 55 μg/ml, Ag NPs were found to be very efficient for preventing biofilm formation.

3.8. Confocal laser scanning electron microscope (CLSM)

The biofilm architecture and live/dead cells of MR-CoNS biofilm in presence and absence of Ag NPs was analyzed by CLSM (Fig. 8a–d). At the BIC of 55 μg/ml, the synthesized Ag NPs are vigorously linked to biofilm producing bacterial receptor and exhibited relatively high intensity green color (AO). In addition, the treated surface topology was observed with collapsed colonies and detachment of the cell receptors due to the interaction of cells upon the NPs treatment (Fig. 8c,d). On the other hand, a clear morphology with sticky nature of the cells was observed in the control image as shown in Fig. 8a,b. In the 2D and 3D data sets are termed in pixels and voxels, respectively. For instance, the x-y images in the z-stack are composed of pixels, whereas the same point in the 3D volume data set is a voxel. The concentration of AO easily absorbed the treated and untreated biofilm forming cells [58]. Previously, an inconsistent biofilm formation of GN uropathogens was observed at 100 μg/ml of actinomycete mediated Ag NPs. It was found to be very efficient at preventing multiplication of biofilm [42]. Hence, our result comparatively proved that the actinomycete mediated Ag NPs are very effective against biofilm bacteria even at a relatively low Ag NPs concentration of 55 μg/ml.

3.9. Scanning electron microscopy (SEM)

The Ag NPs were found to significantly modify the structural variation upon increasing concentration in GPB and GNB, resulting in the destabilization of membrane integrity as established before [59,60]. After dehydration, the flat constitution of cocci shaped morphology was confirmed in untreated control cells (Fig. 8e). On the other hand, the damaged morphology of treated cells with BIC of Ag NPs retaliated surface was clearly exhibited as shown in Fig. 8f. From the results, the cell integrity of bacterial membrane was found to strongly collapse and thereby prone to cellular leakage and subsequently cell death. The arrangement of wrinkle morphology and reduction in membrane integrity of Ag NPs treated MR-CoNS was found to occur at 50 μg/ml BIC as shown by SEM analysis. It revealed that a relatively low concentration of Ag NPs was very effective to trigger biofilm inhibition activity, possibly due to the modified surface morphology of GPB induced by Ag NPs.

4. Conclusion

In the present study, Ag NPs were evaluated as potential antibiofilm candidate. These were successfully synthesized using an eco-friendly biological agent, a biomass of *Nocardiopsis* sp. These Ag NPs were characterized using several systematic analyses, which confirmed that NPs were consistent in size, with an average particles size of 35 nm. The Ag NPs showed 91% of inhibition against biofilm forming MR-CoNS at a concentration as low as 55 μg/ml BIC. Interestingly, Ag NPs decreased the cell viability and increased the intracellular leakage in treated MR-CoNS *S. aureus* when compared with untreated control, accordingly providing a probable mechanism for the improved biological properties of Ag NPs. This was supported by CLSM and SEM microscopic observation. Hence, all the morphological assays evidenced that these synthesized Ag NPs are effective antibacterial drug for MR-CoNS. Hence, our result brings to convey a quality for future drug development and health care settings. Additionally, these findings recommend the use of Ag NPs for the handling of different communicable diseases caused by uropathogens.

Declaration of Competing Interest

All authors declare no conflict of interest.

Acknowledgment

The authors would like to acknowledge the University with Potential for Excellence (UPE) Scheme, Madurai Kamaraj University for generously providing access to UV-visible and FTIR spectroscopy, powder XRD, AFM and SEM instruments facility. The authors also extend their acknowledgment to the Bharathidasan University for providing the University Research fellowship (Ref. No-05441/URF/K7/2013) and for providing access to confocal laser scanning electron microscope (CLSM) (DST-PURSE - Sanction Order No- SR/FT/LS-113/2009) for the entire biological work.

Ethical Consideration

All the samples of this study were approved by the ethics review committee (S. No of IEC Management office: DM/2016/101/55) from the Department of Microbiology, Bharathidasan University, Tiruchirappalli, Tamil Nadu, India. The permission was sought from the hospital and laboratory authorities. The ethical principles of scientific research as well as related national laws and regulations were adhered to.

Appendix A. Supplementary material

Supplementary data to this article can be found online at https://doi.org/10.1016/j.bioorg.2019.103008.

References

[1] U. Rasool, S. Hemalatha, Marine endophytic actinomycetes assisted synthesis of copper nanoparticles (CuNPs): Characterization and antibacterial efficacy against human pathogens, Mater. Lett. 194 (2017) 176–180.
[2] D. Rathod, P. Golinska, M. Wypij, H. Dahm, M.A. Rai, A new report of *Nocardiopsis valliformis* strain OT1 from alkaline Lonar crater of India and its use in synthesis of silver nanoparticles with special reference to evaluation of antibacterial activity and cytotoxicity, Med. Microbiol. Immunol. 205 (2016) 435–447.
[3] G. Rajivgandhi, G. Ramachandran, M. Maruthupandy, S. Saravanakumar, N. Manoharan, Antibacterial effect of endophytic actinomycetes from marine algae against multi drug resistant gram negative bacteria, Exam. Mar. Biol. Oceanogr. 4 (2018) 1–8.
[4] O. Nazl, T. Baygar, C.E. Demirci Domez, O. Dere, A.I. Uysal, A. Aksozek, C. Isik, O. Akturk, Antimicrobial and antibiofilm activity of polyurethane/Hypericum perforatum extrat (PHP) composite, Bioorg Chem. 82 (2019) 224–228.
[5] A. Anila Fariq, T. Khan, A. Yasmin, Microbial synthesis of nanoparticles and their potential applications in biomedicine, J. Appl. Biomed. 15 (2017) 241–248.
[6] G. Rajivgandhi, J. Vijayarani, M. Kannan, A. Murugan, R. Vijayan, N. Manoharan, Isolation and identification of biofilm forming uropathogens from urinary tract infection and its antimicrobial susceptibility pattern, Int. J. Adv. Life. Sci. 7 (2014) 352–363.
[7] R.A. Rane, R. Karpoormath, S.S. Naphade, P. Bangalore, M. Shaikh, G. Hampannavar, Novel synthetic organic compounds inspired from antifeedant marine alkaloids as potent bacterial biofilm inhibitors, Bioorg. Chem. 61 (2015) 66–73.
[8] K. Steffy, G. Shanthi, A.S. Maroky, S. Selvakumar, Enhanced antibacterial effects of green synthesized ZnO NPs using Aristolochia indica against Multi-drug resistant bacterial pathogens from Diabetic Foot Ulcer, J. Infect.Public. Heal. 11 (2018) 463–471.
[9] M. Mahdavi, F. Mavandadnejad, M.H. Yazdi, E. Faghfuri, H. Hashemi, S. Homayouni-Oreh, et al., Oral administration of synthetic selenium nanoparticles induced robust Th1 cytokine pattern after HBs antigen vaccination in mouse model, J. Infect. Public Health 10 (2017) 102–109.
[10] G.C. Shukla, F. Haque, Y. Tor, L.M. Wilhelmsson, J.J. Toulme, H. Isambert, et al., A boost for the emerging field of RNA nanotechnology, ACS Nano 5 (2011) 3405–3418.
[11] S. Iravani, H. Korbekandi, S.V. Mirmohammadi, B. Zolfaghari, Synthesis of silver nanoparticles: chemical, physical and biological methods, Res. Pharm. Sci. 9 (2014) 385–406.
[12] I.Y. Wong, S.N. Bhatia, M. Toner, Nanotechnology: emerging tools for biology and medicine, Genes Dev. 15 (2013) 2397–2408.
[13] G. Jagathesan, P. Rajiv, Biosynthesis and characterization of iron oxide nanoparticles using *Eichhornia crassipes* leaf extract and assessing their antibacterial activity, Biocat. Agricul. Biotech 13 (2008) 90–94.
[14] A. Bicer, P. Taslimi, G. Yakalı, I. Gülçin, M. Serdar Gültekin, G. Turgut Cin, Synthesis, characterization, crystal structure of novel bis thiomethylcyclohexanone derivativs and their inhibitory properties against some metabolic enzymes, Bioorg Chem. 82 (2019) 393–404.
[15] L. Suresh, P. Sagar Vijay Kumar, Y. Poornachandra, C. Ganesh Kumar, G.V.P. Chandramouli, An efficient one pot synthesis of thiochromeno [3,4d] pyrimidines derivativs: inducing ROS dependent antibacterial and anti-biofilm activities, Bioorg. Chem. 68 (2016) 159–165.
[16] G. Yang, Y. Yao, C. Wang, Green synthesis of silver nanoparticles impregnated bacterial cellulose-alginate-composite film with improved properties, Mater. Lett. 209 (2017) 11–14.
[17] A. Devadiga, V.K. Shetty, M.B. Saidutta, Highly stable silver nanoparticles synthesized using *Terminalia catappa* leaves as antibacterial agent and colorimetric mercury sensor, Mater. Lett. 207 (2017) 66–71.
[18] J. Du, T.H. Yi, Biosynthesis of silver nanoparticles by *Variovorax guangxiensis* THG-SQL3 and their antimicrobial potential, Mater. Lett. 178 (2016) 75–78.
[19] D.T. Thuc, T.Q. Huy, L.H. Hoang, B.C. Tien, P.V. Chung, N.T. Thuy, A. TuanLe, Green synthesis of colloidal silver nanoparticles through electrochemical method and their antibacterial activity, Mater. Lett. 181 (2016) 173–177.
[20] A. Hussain, M.F. Alajmi, M.A. Khan, S.A. Pervez, F. Ahmed, S. Amir, F.M. Husain, M.S. Khan, G.M. Shaik, I. Hassan, R.A. Khan, Md.T. Rehman, Biosynthesized silver nanoparticle (agnp) from *Pandanus odorifer* leaf extract exhibits anti-metastasis and anti-biofilm potentials, Front. Microbiol. 10 (2019), https://doi.org/10.3389/fmicb.2019.00008.
[21] H.M. Abd-Elnaby, G.M. Abo-Elala, U.M. Abdel-Raouf, M.M. Hamed, Antibacterial and anticancer activity of extracellular synthesized silver nanoparticles from marine *Streptomyces rochei* MHM13, Egypt. J. Aquat. Res. 42 (2016) 301–312.
[22] A. Samundeeswari, S.P. Dhas, J. Nirmala, S.P. John, A. Mukherjee, N. Chandrasekaran, Biosynthesis of silver nanoparticles using actinobacterium *Streptomyces albogriseolus* and its antibacterial activity, Biotechnol. Appl. Biochem. 59 (2012) 503–507.
[23] M. Maruthupandy, G. Rajivgandhi, Muneeswaran T, Ji-Ming Song, Manoharan N. Biologically synthesized zinc oxide nanoparticles as nanoantibiotics against ESBLs producing gram negative bacteria, Microb. Pathog. 121 (2018) 224–231G.
[24] G. Rajivgandhi, R. Vijayan, M. Kannan, M. Santhanakrishnan, N. Manoharan, Molecular characterization and antibacterial effect of endophytic actinomycetes *Nocardiopsis* sp. GRG1 (KT235640) from brown algae against MDR strains of uropathogens, Bioact. Mater. 1 (2016) 140–150.
[25] M. Goudarzi, S. Seyedjavadi, M.J. Nasiri, H. Goudarzi, R. Sajadi Nia, H. Dabiri, Molecular characteristics of methicillin-resistant *Staphylococcus aureus* (MRSA) strains isolated from patients with bacteremia based on MLST, SCCmec, spa, and agr locus types analysis, Microb. Pathog. 104 (2017) 328–335.
[26] C. Nanoukon, X. Argemi, F. Sogbo, J. Orekan, D. Keller, D. Affolabi, F. Schramm, P. Riegel, L. Baba-Moussa, G. Prévost, Pathogenic features of clinically significant coagulase-negative staphylococci in hospital and community infections in Benin, Int. J. Med. Microbiol. 307 (2017) 75–82.
[27] G. Rajivgandhi, M. Marudupandy, T. Muneeswaran, M. Anand, N. Manoharan, Antibiofilm activity of zinc oxide nanosheets (ZnO NSs) from *Nocardiopsis* sp. GRG1 (KT235640) against MDR strains of gram negative *Proteus mirabilis* and *Escherichia coli*, Process Biochem. 67 (2018) 8–18.
[28] G. Rajivgandhi, M. Marudupandy, G. Ramachandran, M. Priyanga, N. Manoharan, Detection of ESBL genes from ciprofloxacin resistant Gram negative bacteria isolated from urinary tract infections (UTIs), Frontiers Lab. Med. 2 (2018) 5–13.
[29] R. Seng, T. Kitti, R. Thummeepak, P. Kongthai, U. Leungtongkam, S. Wannalerdsakun, S. Sitthisak, Biofilm formation of methicillin-resistant coagulase negative *staphylococci* (MR-CoNS) isolated from community and hospital environments, PLoS ONE 31 (2017) 1–13.
[30] S. Neupane, N.D. Pant, S. Khatiwada, R. Chaudhary, M.R. Banjara, Correlation between biofilm formation and resistance toward different commonly used

antibiotics along with extended spectrum beta lactamase production in uropathogenic *Escherichia coli* isolated from the patients suspected of urinary tract infections visiting Shree Birendra Hospital, Chhauni, Kathmandu, Nepal, Antimicrob. Resist. Infect. Control. 5 (2016) 1–5.
[31] S. Majeed, M.S.B. Abdullah, Anima Nanda, M. Tahir Ansari, In vitro study of the antibacterial and anticancer activities of silver nanoparticles synthesized from *Penicillium brevicompactum* (MTCC-1999), J. Taibah Univ. Sci. 10 (2016) 614–620.
[32] R.D. Wojtyczka, K. Orlewska, M. Kępa, D. Idzik, A. Dziedzic, T. Mularz, M. Krawczyk, M. Miklasińska, T.J. Wąsik, Biofilm formation and antimicrobial susceptibility of *Staphylococcus epidermidis* strains from a hospital environment, Int. J. Environ. Res. Public Health 25 (2014) 4619–4633.
[33] W. Cai, J. Wu, C. Xi, A.J. Ashe, M.E. Meyerhoff, Carboxylebselen- based layer-by-layer films as potential antithrombotic and antimicrobial coatings, Biomaterials 32 (2011) 7774–7784.
[34] U. Manzoor, S. Siddique, R. Ahmed, Z. Noreen, H. Bokhari, I. Ahmad, Antibacterial, Structural and optical characterization of mechano-chemically prepared zno nanoparticles, PLoS ONE 2 (2016) 1–12.
[35] M. Khan, M. Khan, S.F. Adil, M.N. Tahir, W. Tremel, H.Z. Alkhathlan, A. Al-Warthan, M.R. Siddiqui, Green synthesis of silver nanoparticles mediated by *Pulicaria glutinosa* extract, Int. J. Nanomedicine 8 (2013) 1507–1516.
[36] C.K. Nguyen, N.Q. Tran, T.P. Nguyen, D.H. Nguyen, Biocompatible nanomaterials based on dendrimers, hydrogels and hydrogel nanocomposites for use in biomedicine, Adv. Nat. Sci: Nanosci. Nanotechnol. 7 (2016) 1–12.
[37] B. Ajitha, Y. Ashok Kumar Reddy, P. Sreedhara Reddy, H.J. Jeon, C.W. Ahn, Role of capping agents in controlling silver nanoparticles size, antibacterial activity and potential application as optical hydrogen peroxide sensor, RSC Adv. 6 (2016) 36171–36179.
[38] S.S. Shankar, A. Rai, B. Ankamwar, A. Singh, A. Ahmad, M. Sastry, Biological synthesis of triangular gold nanoprisms, Nat. Mater. 3 (2004) 482–488.
[39] M. Josea, S.A. Martin Britto Dhas, Arul Doss Daisy, S. Jerome Das, Synthesis and characterization of nano spheres decorated silver bromide nanorods using a two step chemical reduction route, Optik 127 (2016) 8019–8023.
[40] K. Shameli, M.B. Ahmad, M. Zargar, W.M.Z.W. Yunus, A. Rustaiyan, N.A. Ibrahim, Synthesis of silver nanoparticles in montmorillonite and their antibacterial behavior, Int. J. Nanomed. 6 (2011) 581–590.
[41] G. Rajivgandhi, M. Maruthupandy, N. Manoharan, Detection of TEM and CTX-M genes from ciprofloxacin resistant *Proteus mirabilis* and *Escherichia coli* isolated on urinary tract infections (UTIs), Microb. Pathog. 121 (2018) 123–130.
[42] P.S. Panda, U. Chaudhary, S.K. Dube, Comparison of four different methods for detection of biofilm formation by uropathogens, Ind. J. Pathol. Microbiol. 59 (2016) 177–179.
[43] G. Rajivgandhi, R. Vijayan, M. Maruthupandy, B. Vaseeharan, N. Manoharan, Antibiofilm effect of *Nocardiopsis* sp. GRG 1 (KT235640) compound against biofilm forming Gram negative bacteria on UTIs, Microb. Pathog. 118 (2018) 190–198.
[44] A. Jain, J. Agarwal, S. Bansal, Prevalence of methicillin-resistant, coagulase-negative staphylococci in neonatal intensive care units: findings from a tertiary care hospital in India, J. Med. Microbiol. 53 (2004) 941–944.
[45] H.M. Manukumar, S. Umesha, H.N.N. Kumar, Promising biocidal activity of thymol loaded chitosan silver nanoparticles (T-C@AgNPs) as anti-infective agents against perilous pathogens, Int. J. Biol. Macromol. 102 (2017) 1257–1265.
[46] D. Gupta, A. Singh, A.U. Khan, Nanoparticles as efflux pump and biofilm inhibitor to rejuvenate bactericidal effect of conventional antibiotics, Nanoscale Res. Lett. 12 (2017) 1–6.
[47] S.A. Masurkar, P.R. Chaudhari, V.B. Shidore, S.P. Kamble, Effect of biologically synthesised silver nanoparticles on *Staphylococcus aureus* biofilm quenching and prevention of biofilm formation, IET Nanobiotechnol. 6 (2012) 110–114.
[48] H. Mu, J. Tang, Q. Liu, C. Sun, T. Wang, J. Duan, Potent antibacterial nanoparticles against biofilm and intracellular bacteria, Sci. Rep. 5 (2016) 18877.
[49] M. Altaf, H. Stoeckli-Evans, A. Cuin, D.N. Sato, F.R. Pavan, C. Queico, Synthesis crystal structures, antimicrobial, antifungal and antituberculosis activities of mixed ligand silver (I) complexes, Polyhedron 62 (2013) 138–147.
[50] B. Malaikozhundan, B. Vaseeharan, S. Vijayakumar, R. Sudhakaran, N. Gobi, G. Shanthini, Antibacterial and antibiofilm assessment of *Momordica charantia* fruit extract coated silver nanoparticle, Biocat. Agricul. Biotech. 8 (2016) 189–196.
[51] K. Singh, M. Panghal, S. Kadyan, U. Chaudhary, J.P. Yadav, Antibacterial activity of synthesized silver nanoparticles from *Tinospora cordifolia* against multi drug resistant strains of *Pseudomonas aeruginosa* isolated from burn patients, J. Nanomed. Nanotechnol. 2 (2014) 1–6.
[52] M.A. Perez-Díaz, L. Boegli, G. James, C. Velasquillo, R. Sanchez-Sanchez, R.E. Martínez-Martínez, Silver nanoparticles with antimicrobial activities against *Streptococcus mutans* and their cytotoxic effect, Mater. Sci. Eng. C Mater. Biol. Appl. 55 (2015) 360–366.
[53] A. Panacek, M. Smékalova, R. Večeřová, K. Bogdanová, M. Röderová, M. Kolář, Silver nanoparticles strongly enhance and restore bactericidal activity of inactive antibiotics against multiresistant *Enterobacteriaceae*, Colloids Surf. B Biointerfaces 142 (2016) 392–399.
[54] A. Barapatre, K.R. Aadil, H. Jha Harit, Synergistic antibacterial and antibiofilm activity of silver nanoparticles biosynthesized by lignin-degrading fungus, Bioresour. Bioprocess. 63 (2016) 1–8.
[55] S.T. Appapalam, R. Panchamoorthy, *Aerva lanata* mediated phytofabrication of silver nanoparticles and evaluation of their antibacterial activity against wound associated bacteria, J. Taiwan Inst. Chem. Eng. 78 (2017) 539–551.
[56] G. Rajivgandhi, M. Maruthupandy, T. Veeramani, F. Quero, Wen-Jun Li, Anti-ESBL investigation of chitosan/silver nanocomposites against carbapenem resistant Pseudomonas aeruginosa, Int. J. Biolo. Macromol. 132 (2019) 1221–1234.
[57] J.M. Silvan, I. Zorraquin-Pena, D.G. de Llano, M.V. Moreno-Arribas, J.A. Martinez-Rodriguez, Antibacterial activity of glutathione-stabilized silver nanoparticles against *Campylobacter* multidrug-resistant strains, Front. Microbiol. 9 (2018) 458.
[58] K. Prasad, G.S. Lekshmi, K. Ostrikov, V. Lussini, J. Blinco, M. Mohandas, K. Vasilev, S. Bottle, K. Bazaka, K. Ostrikov, Synergic bactericidal effects of reduced graphene oxide and silver nanoparticles against Gram-positive and Gram-negative bacteria, Sci. Rep. 8 (2017) 1591.
[59] D.J. Fitzgerald, M. Stratford, M.J. Gasson, J. Ueckert, A. Bos, A. Narbad, Mode of antimicrobial action of vanillin against *Escherichia coli*, *Lactobacillus plantarum* and *Listeria innocua*, J. Appl. Microbiol. 97 (2004) 104–113.
[60] E.J. Veldhuizen, J.L. Tjeerdsma-van Bokhoven, C. Zweijtzer, S.A. Burt, H.P. Haagsman, Structural requirements for the antimicrobial activity of carvacrol, J. Agric. Food Chem. 54 (2006) 1874–1879.